Chinese Journal of Aeronautics 25 (2012) 143-154

Contents lists available at ScienceDirect

Chinese Journal of Aeronautics

journal homepage: www.elsevier.com/locate/cja

Flow Stability Model for Fan/Compressors with Annular Duct and Novel Casing Treatment

LIU Xiaohua, SUN Dakun, SUN Xiaofeng*, WANG Xiaoyu

School of Jet Propulsion, Beihang University, Beijing 100191, China

Received 25 March 2011; revised 21 April 2011; accepted 3 June 2011

Abstract

A three-dimensional compressible flow stability model is presented in this paper, which focuses on stall inception of multi-stage axial flow compressors with a finite large radius annular duct configuration for the first time. It is shown that under some assumptions, the stability equation can be obtained yielding from a group of homogeneous equations. The stability can be judged by the non-dimensional imaginary part of the resultant complex frequency eigenvalue. Further more, based on the analysis of the unsteady phenomenon caused by casing treatment, the function of casing treatment has been modeled by a wall impedance condition which is included in the stability model through the eigenvalues and the corresponding eigenfunctions of the system. Finally, some experimental investigation and two numerical evaluation cases are conducted to validate this model and emphasis is placed on numerically studying the sensitivity of the setup of different boundary conditions on the stall inception of axial flow fan/compressors. A novel casing treatment which consists of a backchamber and a perforated plate is suggested, and it is noted that the open area ratio of the casing treatment is less than 10%, and is far smaller than conventional casing treatment with open area ratio of over 50%, which could result in stall margin improvement without obvious efficiency loss of fan/compressors.

Keywords: compressor; stability; rotating stall; casing treatment; eigenvalue

1. Introduction

Considerable work was completed in the past tens of years on investigating the phenomenon of rotating stall of fan/compressors. Since the classical explanation presented by Emmons, et al. [1] in 1955, there have been some developments in the model studies of stall inception. Nenni and Ludwig's work [2] resulted in an analytical expression for the inception condition of two-dimensional incompressible rotating stall, which was later extended to compressible flow in 1979 and a three-dimensional incompressible model without any relevant numerical results reported [3]. Stenning [4] also studied the rotating stall based on a linearized small perturbation analysis in 1980. It is verified that all these models can predict the instability inception condition with a satisfactory accuracy as long as sufficient loss and performance characteristics of the compressors concerned are given. Furthermore, in recent years, more attention is paid to the compressible flow stability of rotating stall in multi-stage compressors. In 1996, X. F. Sun [5] firstly developed a three-dimensional compressible stability model including the effect of the casing treatment, and this work was extended to transonic compressors stability prediction recently [6].

However, most existing works are based on the assumption that the circumferential flow passage comprises of two flat plates which model the hub and tip duct wall of compressors. It should be noted that this assumption implicates an infinite curvature radius, which is an approximate analysis of the actual annular duct. This simplification makes it straightforward to gain the perturbation expression and artificially decompose the radial modes for an eigenvalue. So a

*Corresponding author. Tel.: +86-10-82317408.
E-mail address: sunxf@buaa.edu.cn
Foundation items: National Natural Science Foundation of China (50736007, 50890181); the Innovation Foundation of BUAA for PhD Graduates (300383)

doi: 10.1016/S1000-9361(11)60373-7

model concerning a finite large radius, which searches for an eigenvalue for a coupled multi-radial mode distribution of perturbation in fan/compressors system, should be acceptable and viewed as an improvement towards the real configuration.

On the other hand, casing treatment has long been an effective strategy to meet the requirement of stall margin with the increase of blade loading. Although there were successful practical applications in the research institutions [7-12] and industrial departments [13-14], a large number of different configurations [15-18] were used in various experiments without enough unambiguous or unified explanation. Up to now, most designs of casing treatments have been based on try and error. Smith and Cumpsty [19] admitted that the reason for the effectiveness of casing treatment is not really understood. It was noted that with the discovery of stall precursor in compressors, the idea of a novel casing treatment was proposed by D. K. Sun, et al. [20-21] to suppress the precursor or delay its evolution in order to enhance stall margin. It is obvious that such casing treatment is aimed at affecting stall precursors instead of improving the blade tip flow structure like the conventional casing treatments. So, theoretically it is possible to design a kind of advanced casing treatment with low open area ratio to suppress the stall precursor, which can result in the stall margin improvement without the obvious efficiency loss of fan/compressors.

The present work will introduce a three-dimensional compressible flow stability model of multi-stage compressors with a finite large radius duct, which is obtained by the following steps. First, under the assumptions of uniform mean flow and large radius assumption, the perturbation field is described by linearized Euler equations, which can be solved by mode decomposing plus appropriate boundary condition. Further the compressor stability can be described as an eigenvalue problem, which is established by using the mode-matching technique and applying the conservation law and conditions reflecting the loss characteristics of fan/compressors at the two sides of rotors and stators, which are modeled as a series of actuator disks. Then the eigenvalue equations in matrix form are solved using the winding number integral approach, and the stability can be judged by the non-dimensional imaginary part of the resultant complex frequency eigenvalue. Furthermore, based on the analysis of the unsteady phenomenon caused by casing treatments, the function of casing treatments is modeled by a wall impedance condition which is included in the stability model through the eigenvalues and the corresponding eigenfunctions of the system. Finally, some experimental investigation and two numerical evaluation cases are conducted to validate this model and emphasis is placed on numerically studying the sensitivity of setup of different boundary conditions on the stall inception of axial flow fan/compressors. A novel casing treatment which consists of a backchamber and a perforated plate is suggested, and it is noted that the open area ratio of the casing treatment is less than 10%, far smaller than the conventional casing treatment with open area ratio of over 50%, which could result in stall margin improvement without an obvious efficiency loss of fan/compressors.

2. Theoretical Model of Stall Inception

2.1. Governing equations and pressure perturbation

In the present work, a linear cascade of blades is modeled by the three-dimensional actuator disk. The actual compressor configuration is simplified as uniform annular duct with finite large radius, and the radial mean flow is ignored. A three-dimensional, compressible, inviscid, non-heat-conductive flow is considered. The governing equations for a small disturbance problem are the linearized Euler equations as follows, which reflect the conservation relations for mass, momentum and energy.

$$\frac{\partial \rho'}{\partial t}+\rho_0\frac{\partial (r\,v_r')}{r\partial r}+\rho_0\frac{\partial v_\theta'}{r\partial\theta}+V_0\frac{\partial \rho'}{r\partial\theta}+\rho_0\frac{\partial v_x'}{\partial x}+U_0\frac{\partial \rho'}{\partial x}=0 \tag{1}$$

$$\frac{\partial v_r'}{\partial t}+V_0\frac{\partial v_r'}{r\partial\theta}+U_0\frac{\partial v_r'}{\partial x}-2V_0\frac{v_\theta'}{r}=-\frac{1}{\rho_0}\cdot\frac{\partial p'}{\partial r} \tag{2}$$

$$\frac{\partial v_\theta'}{\partial t}+V_0\frac{\partial v_\theta'}{r\partial\theta}+U_0\frac{\partial v_\theta'}{\partial x}+V_0\frac{v_r'}{r}=-\frac{1}{\rho_0}\cdot\frac{\partial p'}{r\partial\theta} \tag{3}$$

$$\frac{\partial v_x'}{\partial t}+V_0\frac{\partial v_x'}{r\partial\theta}+U_0\frac{\partial v_x'}{\partial x}=-\frac{1}{\rho_0}\cdot\frac{\partial p'}{\partial x} \tag{4}$$

$$\frac{\partial p'}{\partial t}+V_0\frac{\partial p'}{r\partial\theta}+U_0\frac{\partial p'}{\partial x}=k\frac{p_0}{\rho_0}\left(\frac{\partial \rho'}{\partial t}+V_0\frac{\partial \rho'}{r\partial\theta}+U_0\frac{\partial \rho'}{\partial x}\right) \tag{5}$$

where ρ is density, U and V are the velocity components, p is the pressure, k the specific heat ratio, and v the fluctuating velocity. The subscript "0" represents the mean flow, while the superscript "′ " represents perturbation. x, r and θ represent axial, radial and circumferential coordinates, respectively. A large radius assumption is made that the curvature radius r_{m} of annular duct is not infinite but much greater than the axial perturbation wavelength λ_x:

$$\lambda_x \ll r_{\mathrm{m}} \ll +\infty \tag{6}$$

Given that most previous stability models consider the actual annular duct as rectangular channel, i.e., infinite curvature radius, a model concerning a finite radius should be acceptable and viewed as an improvement. Under this condition, all items including V_0 become high-level minim in each equation and can be omitted. The simplified equations are obtained as follows:

$$\frac{\partial \rho'}{\partial t}+\rho_0\frac{\partial (r\,v_r')}{r\partial r}+\rho_0\frac{\partial v_\theta'}{r\partial\theta}+\rho_0\frac{\partial v_x'}{\partial x}+U_0\frac{\partial \rho'}{\partial x}=0 \tag{7}$$

$$\frac{\partial v_x'}{\partial t}+U_0\frac{\partial v_x'}{\partial x}=-\frac{1}{\rho_0}\cdot\frac{\partial p'}{\partial x} \tag{8}$$

$$\frac{\partial v_r'}{\partial t}+U_0\frac{\partial v_r'}{\partial x}=-\frac{1}{\rho_0}\cdot\frac{\partial p'}{\partial r} \tag{9}$$

$$\frac{\partial v_\theta'}{\partial t}+U_0\frac{\partial v_\theta'}{\partial x}=-\frac{1}{\rho_0}\cdot\frac{\partial p'}{r\partial\theta} \tag{10}$$

$$\frac{\partial p'}{\partial t}+U_0\frac{\partial p'}{\partial x}=k\frac{p_0}{\rho_0}\left(\frac{\partial \rho'}{\partial t}+U_0\frac{\partial \rho'}{\partial x}\right) \tag{11}$$

From Eqs. (7)-(11), it can be shown that fluctuating variables related to pressure satisfy the wave equation in the form of

$$(1-Ma_x{}^2)\frac{\partial^2 p'}{\partial x^2}+\frac{\partial^2 p'}{r^2\partial\theta^2}+\frac{\partial^2 p'}{\partial r^2}-\frac{1}{a_0{}^2}\cdot\frac{\partial^2 p'}{\partial t^2}-\frac{2Ma_x}{a_0}\cdot\frac{\partial^2 p'}{\partial x\partial t}+\frac{\partial p'}{r\partial r}=0 \tag{12}$$

where Ma_x is the axial Mach number, a_0 the sound speed. Assume the solution of Eq. (12) is

$$p'(x,r,\theta,t)=\sum_{m=-\infty}^{+\infty}\sum_{n=1}^{+\infty}\overline{p}_{mn}\Psi_{mn}(r)\,\mathrm{e}^{\mathrm{i}(m\theta+\omega t+\alpha_{mn}x)} \tag{13}$$

where m is the circumferential mode number, or ordinal number of harmonic, n the radial mode number, ω the eigenfrequency, α_{mn} the axial wave number, and $\overline{p}_{mn}$ the wave amplitude. Substituting Eq. (13) into Eq. (12) yields an equation about the radial eigenfunction $\Psi_{mn}(r)$:

$$r^2\frac{\partial^2\Psi_{mn}(r)}{\partial r^2}+r\frac{\partial\Psi_{mn}(r)}{\partial r}+\left\{\left[\left(\frac{\omega}{a_0}+Ma_x\alpha_{mn}\right)^2-\alpha_{mn}{}^2\right]r^2-m^2\right\}\Psi_{mn}(r)=0 \tag{14}$$

Assume the solution of Eq. (14) is

$$\Psi_{mn}(r)=b_{mn1}\mathrm{J}_m(\mu_{mn}r)+b_{mn2}\mathrm{N}_m(\mu_{mn}r) \tag{15}$$

where $\mathrm{J}_m(\mu_{mn}r)$ and $\mathrm{N}_m(\mu_{mn}r)$ are Bessel functions of the first and second kind, respectively, b_{mn1} and b_{mn2} are two undetermined coefficients, and μ_{mn} is the radial wave number. For hard wall boundary condition on both hub and tip wall,

$$\left.\frac{\partial\Psi_{mn}(r)}{\partial r}\right|_{r=r_\mathrm{h},\,r_\mathrm{t}}=0 \tag{16}$$

where r_h and r_t are the radius at hub and tip, respectively.

So the radial wave number for hard wall can be solved by the following equations:

$$\begin{cases}b_{mn1}\dfrac{\partial}{\partial r}(\mathrm{J}_m(\mu_{mn}r_\mathrm{h}))+b_{mn2}\dfrac{\partial}{\partial r}(\mathrm{N}_m(\mu_{mn}r_\mathrm{h}))=0\\ b_{mn1}\dfrac{\partial}{\partial r}(\mathrm{J}_m(\mu_{mn}r_\mathrm{t}))+b_{mn2}\dfrac{\partial}{\partial r}(\mathrm{N}_m(\mu_{mn}r_\mathrm{t}))=0\end{cases} \tag{17}$$

where the undetermined coefficients b_{mn1} and b_{mn2} cannot be zero at the same time for a nontrivial solution, so

$$\begin{vmatrix}\dfrac{\partial}{\partial r}(\mathrm{J}_m(\mu_{mn}r_\mathrm{h})) & \dfrac{\partial}{\partial r}(\mathrm{N}_m(\mu_{mn}r_\mathrm{h}))\\ \dfrac{\partial}{\partial r}(\mathrm{J}_m(\mu_{mn}r_\mathrm{t})) & \dfrac{\partial}{\partial r}(\mathrm{N}_m(\mu_{mn}r_\mathrm{t}))\end{vmatrix}=0 \tag{18}$$

Meanwhile, the axial wave number α_{mn} is solved in the above process. The complete expression for pressure perturbation is

$$p'(x,r,\theta,t)=\sum_{m=-\infty}^{+\infty}\sum_{n=1}^{+\infty}(\overline{p}_{mn}^{+j}\mathrm{e}^{\mathrm{i}\alpha_{mn}^{+j}(x-x^j)}\Psi_{mn}^{+j}(r)+\overline{p}_{mn}^{-j}\mathrm{e}^{\mathrm{i}\alpha_{mn}^{-j}(x-x^j)}\Psi_{mn}^{-j}(r))\mathrm{e}^{\mathrm{i}(m\theta+\omega t)} \tag{19}$$

where x^j is the axial coordinates for an arbitrary reference plane; "$+j$" and "$-j$" represent the waves traveling downstream and upstream from the plane x^j, respectively. After substituting Eq. (19) into Eqs. (8)-(11), the other perturbation corresponding to pressure can be obtained.

$$v_{\mathrm{px}}'(x,r,\theta,t)=-\sum_{m=-\infty}^{+\infty}\sum_{n=1}^{+\infty}\frac{1}{\rho_0^j}\left(\frac{\overline{p}_{mn}^{+j}\alpha_{mn}^{+j}\mathrm{e}^{\mathrm{i}\alpha_{mn}^{+j}(x-x^j)}}{\omega+U_0^j\alpha_{mn}^{+j}}\Psi_{mn}^{+j}(r)+\frac{\overline{p}_{mn}^{-j}\alpha_{mn}^{-j}\mathrm{e}^{\mathrm{i}\alpha_{mn}^{-j}(x-x^j)}}{\omega+U_0^j\alpha_{mn}^{-j}}\Psi_{mn}^{-j}(r)\right)\mathrm{e}^{\mathrm{i}(m\theta+\omega t)} \tag{20}$$

$$v_{\mathrm{pr}}'(x,r,\theta,t)=\sum_{m=-\infty}^{+\infty}\sum_{n=1}^{+\infty}\frac{\mathrm{i}}{\rho_0^j}\left(\frac{\overline{p}_{mn}^{+j}\mathrm{e}^{\mathrm{i}\alpha_{mn}^{+j}(x-x^j)}}{\omega+U_0^j\alpha_{mn}^{+j}}\phi_{mn}^{+j}(r)+\frac{\overline{p}_{mn}^{-j}\mathrm{e}^{\mathrm{i}\alpha_{mn}^{-j}(x-x^j)}}{\omega+U_0^j\alpha_{mn}^{-j}}\phi_{mn}^{-j}(r)\right)\mathrm{e}^{\mathrm{i}(m\theta+\omega t)} \tag{21}$$

$$v_{\mathrm{p}\theta}'(x,r,\theta,t)=-\sum_{m=-\infty}^{+\infty}\sum_{n=1}^{+\infty}\frac{1}{\rho_0^j r}\left(\frac{m\overline{p}_{mn}^{+j}\mathrm{e}^{\mathrm{i}\alpha_{mn}^{+j}(x-x^j)}}{\omega+U_0^j\alpha_{mn}^{+j}}\Psi_{mn}^{+j}(r)+\frac{m\overline{p}_{mn}^{-j}\mathrm{e}^{\mathrm{i}\alpha_{mn}^{-j}(x-x^j)}}{\omega+U_0^j\alpha_{mn}^{-j}}\Psi_{mn}^{-j}(r)\right)\mathrm{e}^{\mathrm{i}(m\theta+\omega t)} \tag{22}$$

$$\rho_{\mathrm{p}}'(x,r,\theta,t)=\sum_{m=-\infty}^{+\infty}\sum_{n=1}^{+\infty}\frac{1}{(a_0^j)^2}\left(\overline{p}_{mn}^{+j}\mathrm{e}^{\mathrm{i}\alpha_{mn}^{+j}(x-x^j)}\Psi_{mn}^{+j}(r)+\overline{p}_{mn}^{-j}\mathrm{e}^{\mathrm{i}\alpha_{mn}^{-j}(x-x^j)}\Psi_{mn}^{-j}(r)\right)\mathrm{e}^{\mathrm{i}(m\theta+\omega t)} \tag{23}$$

where ϕ_{mn} is the deriative of Ψ_{mn}.

2.2. Vortex wave

Since the vortex wave will not cause the pressure

variation, the solutions related to vortex mode can be given by the homogeneous form of Eqs. (8)-(10). It is noted that v_r is composed of two parts: one is the contribution by the pressure wave v_{pr} and the other one is by the vortex wave v_{vr}. Since the wave lengths of the pressure wave and the vortex wave are different from each other, v_{vr} can be assumed not to contribute to the left-hand side of Eq. (16). For this reason, v_{vr} is concluded to satisfy the following condition on solid wall:

$$v_{\mathrm{vr}}'|_{r=r_{\mathrm{h}},\,r_{\mathrm{t}}}=0 \tag{24}$$

In the similar way, the corresponding solutions for the homogeneous form of Eqs. (8)-(10) are

$$v_{\mathrm{vx}}'(x,r,\theta,t)=\sum_{m=-\infty}^{+\infty}\sum_{n=1}^{+\infty}\overline{v}_{\mathrm{vx}mn}^{+j}\Psi_{\mathrm{v}mn}^{+j}(r)\mathrm{e}^{\mathrm{i}(m\theta+\omega t)}\mathrm{e}^{-\mathrm{i}\frac{\omega}{U_0^j}(x-x^j)} \tag{25}$$

$$v_{\mathrm{vr}}'(x,r,\theta,t)=\sum_{m=-\infty}^{+\infty}\sum_{n=1}^{+\infty}\overline{v}_{\mathrm{vr}mn}^{+j}\phi_{\mathrm{v}mn}^{+j}(r)\mathrm{e}^{\mathrm{i}(m\theta+\omega t)}\mathrm{e}^{-\mathrm{i}\frac{\omega}{U_0^j}(x-x^j)} \tag{26}$$

$$v_{\mathrm{v}\theta}'(x,r,\theta,t)=\sum_{m=-\infty}^{+\infty}\sum_{n=1}^{+\infty}\overline{v}_{\mathrm{v}\theta mn}^{+j}\Psi_{\mathrm{v}mn}^{+j}(r)\mathrm{e}^{\mathrm{i}(m\theta+\omega t)}\mathrm{e}^{-\mathrm{i}\frac{\omega}{U_0^j}(x-x^j)} \tag{27}$$

where $\overline{v}_{\mathrm{vx}mn}^{+j}$, $\overline{v}_{\mathrm{vr}mn}^{+j}$ and $\overline{v}_{\mathrm{v}\theta mn}^{+j}$ are the wave amplitudes, the eigenfunctions are

$$\Psi_{\mathrm{v}mn}^{+j}(r)=b_{mn1}\mathrm{J}_m(\mu_{\mathrm{v}mn}^{+j}r)+b_{mn2}\mathrm{N}_m(\mu_{\mathrm{v}mn}^{+j}r) \tag{28}$$

$$\phi_{\mathrm{v}mn}^{+j}(r)=b_{mn1}\frac{\partial}{\partial r}(\mathrm{J}_m(\mu_{\mathrm{v}mn}^{+j}r))+b_{mn2}\frac{\partial}{\partial r}(\mathrm{N}_m(\mu_{\mathrm{v}mn}^{+j}r)) \tag{29}$$

2.3. Entropy wave

Since the entropy and the vorticity are related by Crocco's theorem, there must be the solution of the entropy wave with the solution of the vorticity wave inside the gap. On the other hand, it can be shown that the entropy wave relates to a density fluctuation, or, to temperature fluctuation since no pressure fluctuation is accompanied by this wave. So according to energy equation, the density related to entropy variation will be determined by the equation:

$$\frac{\partial\rho'}{\partial t}+U_0\frac{\partial\rho'}{\partial x}=0 \tag{30}$$

Furthermore, the walls are assumed to be adiabatic to such fluctuation, so the adiabatic condition of boundary walls is described as

$$\left.\frac{\partial T}{\partial r}\right|_{r=r_{\mathrm{h}},\,r_{\mathrm{t}}}=0 \tag{31}$$

where T is the temperature.

The solution of Eq. (30) is

$$\rho_{\mathrm{v}}'(x,r,\theta,t)=\sum_{m=-\infty}^{+\infty}\sum_{n=1}^{+\infty}\overline{\rho}_{\mathrm{v}mn}^{+j}\Psi_{\mathrm{v}mn}^{+j}(r)\mathrm{e}^{\mathrm{i}(m\theta+\omega t)}\mathrm{e}^{-\mathrm{i}\frac{\omega}{U_0^j}(x-x^j)} \tag{32}$$

where $\overline{\rho}_{\mathrm{v}mn}^{+j}$ is the wave amplitude.

2.4. Complete solution of perturbation

With the above basic solutions, it is shown that pressure perturbation is

$$p'^j(x,r,\theta,t)=\sum_{m=-\infty}^{+\infty}\sum_{n=1}^{+\infty}\Big(\overline{p}_{mn}^{+j}\mathrm{e}^{\mathrm{i}\alpha_{mn}^{+j}(x-x^j)}\Psi_{mn}^{+j}(r)+\overline{p}_{mn}^{-j}\mathrm{e}^{\mathrm{i}\alpha_{mn}^{-j}(x-x^j)}\Psi_{mn}^{-j}(r)\Big)\mathrm{e}^{\mathrm{i}(m\theta+\omega t)} \tag{33}$$

Density perturbation is

$$\rho'^j(x,r,\theta,t)=\sum_{m=-\infty}^{+\infty}\sum_{n=1}^{+\infty}\left[\frac{1}{(a_0^j)^2}(\overline{p}_{mn}^{+j}\mathrm{e}^{\mathrm{i}\alpha_{mn}^{+j}(x-x^j)}\Psi_{mn}^{+j}(r)+\overline{p}_{mn}^{-j}\mathrm{e}^{\mathrm{i}\alpha_{mn}^{-j}(x-x^j)}\Psi_{mn}^{-j}(r))+\overline{\rho}_{\mathrm{v}mn}^{+j}\Psi_{\mathrm{v}mn}^{+j}(r)\mathrm{e}^{-\mathrm{i}\frac{\omega}{U_0^j}(x-x^j)}\right]\mathrm{e}^{\mathrm{i}(m\theta+\omega t)} \tag{34}$$

Axial velocity perturbation is

$$v_x'^j(x,r,\theta,t)=\sum_{m=-\infty}^{+\infty}\sum_{n=1}^{+\infty}\left[-\frac{1}{\rho_0^j}\left(\frac{\overline{p}_{mn}^{+j}\alpha_{mn}^{+j}\mathrm{e}^{\mathrm{i}\alpha_{mn}^{+j}(x-x^j)}}{\omega+U_0^j\alpha_{mn}^{+j}}\Psi_{mn}^{+j}(r)+\frac{\overline{p}_{mn}^{-j}\alpha_{mn}^{-j}\mathrm{e}^{\mathrm{i}\alpha_{mn}^{-j}(x-x^j)}}{\omega+U_0^j\alpha_{mn}^{-j}}\Psi_{mn}^{-j}(r)\right)+\overline{v}_{\mathrm{vx}mn}^{+j}\Psi_{\mathrm{v}mn}^{+j}(r)\mathrm{e}^{-\mathrm{i}\frac{\omega}{U_0^j}(x-x^j)}\right]\mathrm{e}^{\mathrm{i}(m\theta+\omega t)} \tag{35}$$

Radial velocity perturbation is

$$v_r'^j(x,r,\theta,t)=\sum_{m=-\infty}^{+\infty}\sum_{n=1}^{+\infty}\left[\frac{\mathrm{i}}{\rho_0^j}\left(\frac{\overline{p}_{mn}^{+j}\mathrm{e}^{\mathrm{i}\alpha_{mn}^{+j}(x-x^j)}}{\omega+U_0^j\alpha_{mn}^{+j}}\phi_{mn}^{+j}(r)+\frac{\overline{p}_{mn}^{-j}\mathrm{e}^{\mathrm{i}\alpha_{mn}^{-j}(x-x^j)}}{\omega+U_0^j\alpha_{mn}^{-j}}\phi_{mn}^{-j}(r)\right)+\overline{v}_{\mathrm{vr}mn}^{+j}\phi_{\mathrm{v}mn}^{+j}(r)\mathrm{e}^{-\mathrm{i}\frac{\omega}{U_0^j}(x-x^j)}\right]\mathrm{e}^{\mathrm{i}(m\theta+\omega t)} \tag{36}$$

Circumferential velocity perturbation is

$$v_\theta'^j(x,r,\theta,t)=\sum_{m=-\infty}^{+\infty}\sum_{n=1}^{+\infty}\left[-\frac{1}{\rho_0^j r}\left(\frac{m\overline{p}_{mn}^{+j}\mathrm{e}^{\mathrm{i}\alpha_{mn}^{+j}(x-x^j)}}{\omega+U_0^j\alpha_{mn}^{+j}}\cdot\Psi_{mn}^{+j}(r)+\frac{m\overline{p}_{mn}^{-j}\mathrm{e}^{\mathrm{i}\alpha_{mn}^{-j}(x-x^j)}}{\omega+U_0^j\alpha_{mn}^{-j}}\Psi_{mn}^{-j}(r)\right)+\overline{v}_{\mathrm{v}\theta mn}^{+j}\Psi_{\mathrm{v}mn}^{+j}(r)\mathrm{e}^{-\mathrm{i}\frac{\omega}{U_0^j}(x-x^j)}\right]\mathrm{e}^{\mathrm{i}(m\theta+\omega t)} \tag{37}$$

In gap flow region, there are five mode coefficients for one specific mode (m, n).

2.5. Mode-matching equations

The coefficients of perturbation wave in adjacent gap regions are coupled via five mode matching conditions in the blade reference frame, which reflect some conservation law and the loss characteristics of multi-stage compressors at the two sides of rotors or stators modeled as a series of actuator disks.

1) Mass conservation

$$\rho'^{j}U_0^j+\rho_0^j v_x'^j=\rho'^{j+1}U_0^{j+1}+\rho_0^{j+1}v_x'^{j+1} \tag{38}$$

2) Continuity of radial velocity

$$v_r'^j=v_r'^{j+1} \tag{39}$$

3) Conservation of rothalpy

$$-\frac{(a_0^j)^2}{k-1}\cdot\frac{\rho'^j}{\rho_0^j}+\frac{k}{k-1}\cdot\frac{p'^j}{\rho_0^j}+U_0^j v_x'^j+(V_0{}^j+\Omega^j r)v_\theta'^j=$$
$$-\frac{(a_0^{j+1})^2}{k-1}\cdot\frac{\rho'^{j+1}}{\rho_0^{j+1}}+\frac{k}{k-1}\cdot\frac{p'^{j+1}}{\rho_0^{j+1}}+U_0^{j+1}v_x'^{j+1}+$$
$$(V_0{}^{j+1}+\Omega^j r)v_\theta'^{j+1} \tag{40}$$

where Ω is the rotational speed of rotor and the rothalpy is defined as

$$I=\frac{k}{k-1}\cdot\frac{p}{\rho}+\frac{1}{2}v_{\mathrm{w}}{}^2-\frac{1}{2}r^2\Omega^2 \tag{41}$$

where v_{w} is the relative speed.

4) Kutta condition

The Kutta condition states that both the steady and unsteady flows must be aligned with the blades at the trailing edges, which leads to the equation

$$U_0^{j+1}v_\theta'^{j+1}=(\Omega^j r+V_0^{j+1})v_x'^{j+1} \tag{42}$$

5) Relative total pressure loss characteristics

The total pressure loss is assumed to occur through each actuator disk. This relation is matched through the total loss coefficient ξ_{s}^j which is assumed by a function relationship $\xi_{\mathrm{s}}^j=\xi_{\mathrm{qs}}^j\tan\beta^j$ in a quasi-steady manner as a function of the inlet relative flow angle β^j. Its derivative to β^j is defined as $\mathrm{d}\xi_{\mathrm{s}}^j$.

$$\xi_{\mathrm{s}}^j=\frac{p_{\mathrm{t}}^j-p_{\mathrm{t}}^{j+1}}{\rho^j(v_{\mathrm{w}}^j)^2/2} \tag{43}$$

$$\mathrm{d}\xi_{\mathrm{s}}^j=\frac{\partial\xi_{\mathrm{s}}^j}{\partial\tan\beta^j} \tag{44}$$

where p_{t} is the relative total pressure.

The first-order lag equation is used herein to find the dynamic loss response in the form of

$$\tau\frac{\partial\xi_{\mathrm{s}}^j}{\partial t}=\xi_{\mathrm{qs}}^j-\xi_{\mathrm{s}}^j \tag{45}$$

where τ is the time lag. The numerical results for three different time lags do not show change qualitatively, so the time lag used in this work is simply set to be the time for the mean flow passing through the blade row. Then it is shown that the total pressure loss relation is

$$p_{\mathrm{t}}'^j-p_{\mathrm{t}}'^{j+1}=\frac{1}{1+\mathrm{i}\omega\tau}\left[\xi_{\mathrm{s}}^j\rho'^j\frac{(v_{\mathrm{w}}^j)^2}{2}+\mathrm{d}\xi_{\mathrm{s}}^j\Delta\tan\beta^j\cdot\right.$$
$$\left.\rho_0^j\frac{(v_{\mathrm{w}}^j)^2}{2}+\xi_{\mathrm{s}}^j\rho_0^j(U_0^j v_x'^j+(\Omega^j r+V_0^j)v_\theta'^j)\right] \tag{46}$$

2.6. Closure of stability equation

Since there is no coupling between each circumferential harmonic wave, consideration is restricted to a particular circumferential mode number "*m*" and limited radial mode number "*N*", then there are 5*N* unknown coefficients in description of the gap flow fields. Assume that there are no inlet disturbances caused by entropy or vortex and no reflection, this inlet condition yields

$$\begin{cases}\overline{p}_{mn}^{+1}=0 & \overline{\rho}_{\mathrm{v}mn}^{+1}=0\\ \overline{v}_{\mathrm{v}\theta mn}^{+1}=0 & \overline{v}_{\mathrm{v}rmn}^{+1}=0\end{cases}\quad(n=1,2,\cdots,N) \tag{47}$$

For the outlet of the blade row, assuming that there is no reflection, then

$$\overline{p}_{mn}^{-(k+1)}=0\quad(n=1,2,\cdots,N) \tag{48}$$

Given that consideration is given to *K* cascades, a specific circumferential mode number *m* and primary *N* radial modes, there are 5*KN* unknown variables left. And applying 5 matching equations on *K* cascades and *N* integral matching conditions leads to 5*KN* closed equations which are described in matrix form of

$$[\boldsymbol{G}_{mN}(\omega)]_{5KN\times5KN}\begin{bmatrix}\boldsymbol{\Upsilon}_1\\ \boldsymbol{\Upsilon}_2\\ \vdots\\ \boldsymbol{\Upsilon}_N\end{bmatrix}_{5KN}=\boldsymbol{0} \tag{49}$$

where all unknown mode coefficients are arranged in one column vector $\boldsymbol{\Upsilon}$.

Since Eq. (45) is homogeneous, a non-trivial solution exists if

$$\det(\boldsymbol{G}_{mN}(\omega))=0 \tag{50}$$

Solving the established eigenvalue problem Eq. (50) leads to the resultant complex frequency $\omega=\omega_{\mathrm{r}}+\mathrm{i}\omega_{\mathrm{i}}$. The imaginary part of ω represents whether the system is stable with positive value or unstable with negative value, and the real part of ω determines the rotating frequency of the precursor wave. The two nondimensional parts are defined as relative velocity and damping factor as follows:

$$\text{Relative velocity}=\frac{\omega_{\mathrm{r}}}{2m\pi f} \tag{51}$$

$$\text{Damping factor}=\frac{r\omega_{\mathrm{i}}}{mU_0} \tag{52}$$

2.7. Numerical method for solving stability equation

In the present investigation, winding number integral approach is applied to solving the stability Eq. (50). It is demonstrated that this method has advantages over other methods that have been proposed, Raphson-Newton iteration methods in particular. More of details the method are presented in Ref. [20] and Refs. [22]-[23]. The authors also adopt singular value decomposition (SVD) method in matrix theory over a fine grid on the complex plane, and find that similar accuracy can be derived with a little longer time expended.

3. Stability Model Including the Effect of Casing Treatment

3.1. Unsteady mechanism of casing treatment

In Ref. [20], a complete theory based on vortex wave interaction is made to explain the unsteady mechanism of a novel casing treatment. By applying vortex sound theory, Bechert [24] and Howe [25-26] further explained the phenomenon and set up the theoretical model to calculate the absorptive properties of a perforated screen with bias flow, and their investigations all show that a perforated plate with bias flow will not only change the impedance condition but also the range of absorption frequency by adjusting the bias flow. For a recess casing treatment, when the radial flow enters the cavity from the blade tip and blow ahead of the blade inlet, the vortex shedding will happen as described in Fig. 1. A noticeable fact is that the wall boundary condition will change greatly. Physically, one of the approaches to describe unsteady boundary is to use "impedance" concept [25].

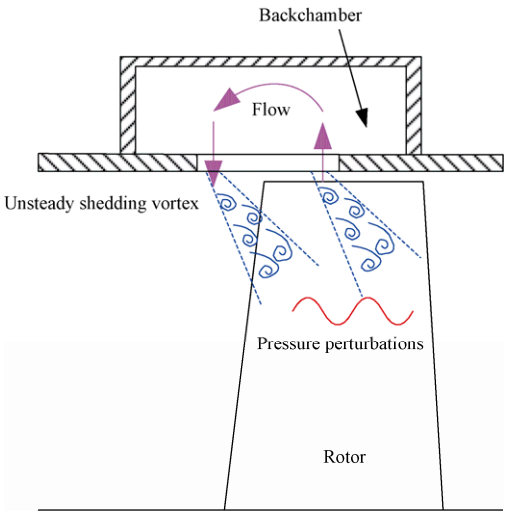

Fig.1 Schematic of vortex wave interaction in casing treatment.

The physical explanations of the above phenomenon is that when a pressure disturbance interacts with a hole and slot with the mean flow through them, unsteady vortex ring or vortex street will be formed due to the requirement of the edge condition, then the energy exchange between the pressure wave and vortex wave will remarkably change the wall boundary condition. The above analysis further shows that if we design a casing treatment as displayed in Fig. 1, an unsteady boundary condition will naturally be formed. In fact, lots of models [27-30] developed on the basis of vortex method were also validated by different experiments [31].

3.2. Mathematical model of casing treatment

As we know, the stability of a system is determined by its initial and boundary conditions, and any change of the boundary condition will inevitably lead to the influence on its stability. Because of this, it could be clearly concluded that the unsteady impedance boundary condition caused by the recirculating flow in the casing treatment will certainly have an influence on the generation and development of initial perturbation. Therefore, how to describe and include the effect of the novel casing treatment in a three-dimensional stability model is the key to determine the design parameters of casing treatment for practical applications, and a reasonable parameter combination is derived by the study of boundary sensitivity on the stall inception under some restrictions.

For the simplification of physical problem, we assume that a casing treatment is right ahead of a compressor with a neglectable distance as shown in Fig. 2. Although there is only one rotor blade row in this figure, the compressors with one stage or multi-stage can also be modeled by applying the relevant matching conditions on the interface.

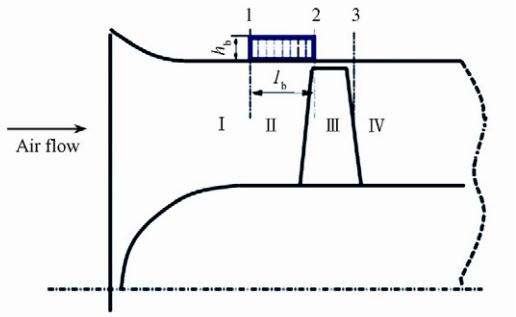

Fig. 2 Schematic of a single blade row and a new type of casing treatment.

In the present work, equivalent surface source method is applied to modeling the impedance boundary, and a unified model which can account for the effect of casing treatment is established. Equivalent surface source method was firstly verified by Namba and Fukushige [32], and developed by X. F. Sun, et al. [33] in the configuration shown in Fig. 3.

After applying impedance definition and Rayleigh conductivity concept which can be calculated by impedance model [30], the integral transformation along the axial direction is conducted to turn the integral

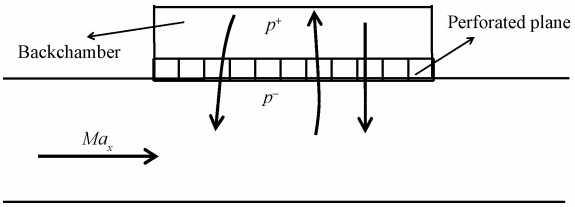

Fig. 3 Schematic of a duct with perforated plate and back-chamber.

equation into an algebraic equation without a special treatment to the singularity problem which is met by Namba and Fukushige [32]. More details about mathematical model of casing treatment is given by Ref. [33]. Finally, with the model for the casing treatment described above, two new equations are obtained by using the continuity of pressure and velocity at both ends of the casing treatment. Then these new equations are combined into the previous coefficient matrix of eigenvalue equations for solid boundary condition. So, the final stability model is improved to corporate the effect of this novel casing treatment on the stall inception.

4. Numerical Prediction Results and Discussion

In this part, two numerical cases are conducted to validate the developed model, which firstly focus on the stall inception prediction for solid boundary and then the sensitivity of casing treatment on the stability of fan/compressors. It is noted that for a flow stability problem, the lower order circumferential modes always tend to be unstable firstly compared to the higher order modes. So, in this paper, emphasis is put on the most unstable mode and how to stabilize this mode.

4.1. NASA Rotor 37 at 70% design rotational speed

4.1.1. Stall inception's prediction

The first validation of this model is to predict the inception of rotating stall for a typical high speed compressor in subsonic case, i.e., NASA Rotor 37 at 70% design rotational speed. The data from experiment at this rotational speed is used as the input parameters, and the inlet relative Mach number is between 0.8 and 1.0. More details of the geometries and characteristics of this rotor can be referred to NASA report given by Moore and Reid [34]. Figure 4 shows the relative speed and damping factor of the perturbation frequency in inception period of instability.

As shown in Fig. 4(a) and Fig. 4(b), there are two lines, which represent the two different circumferential modes m=1 and m=2, respectively. It is seen from Fig. 4(a) that the dimensionless perturbation velocity in inception period of rotating stall ranges from 0.6 to 0.7 for the two modes.

Along with the throttling process, the damping factor decreases gradually and becomes negative at some specific point of lower mass flow rate coefficient

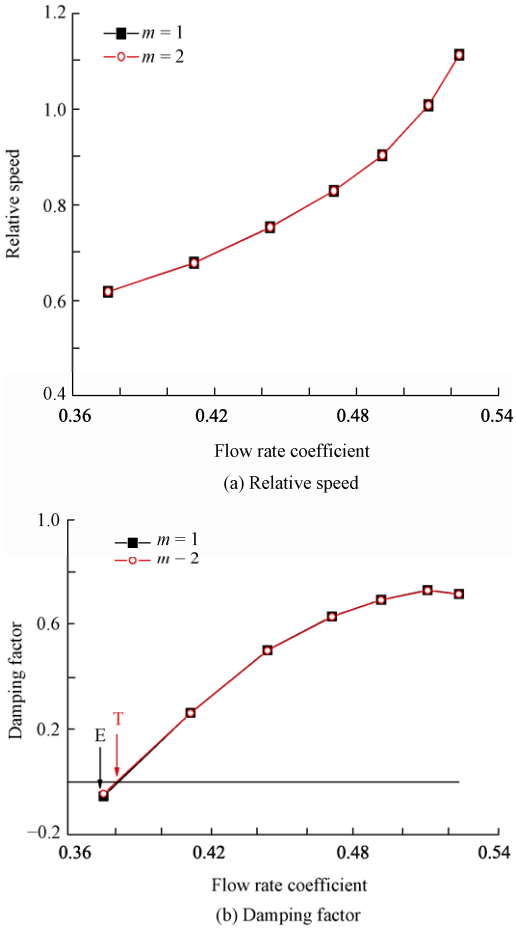

Fig. 4 Stability prediction of NASA Rotor 37 at 70% design rotational speed.

which means the occurrence of compressor instability. The arrow labeled by "E" in Fig. 4(b) denotes the experimental onset point of rotating stall, while that labeled by "T" points to the onset point predicted by the model. The difference of flow rate coefficient between theory and experiment is about 0.01, while the relative error is less than 3%. It is not known from the experiment which mode contributes to the inception point of rotating stall. From our theoretical prediction, the two different circumferential modes seem to pass through the neutral point at the same time. This investigation shows that the present model is capable of predicting the stall inception for high subsonic rotor.

It should be noted that at the beginning of throttling, NASA Rotor 37 exhibits precursor waves with a relative speed of approximately or appreciably higher than the rotor rotation. To the authors' knowledge, some finding of the kind was discovered experimentally. Tryfonidis, et al. [35] conducted many experiments on eight different high speed compressors with identical processing, and two types of behavior of precursor waves occurred prior to stall. Apart from some waves with a rotation frequency of approximately one-half the rotor speed and a wavelength which is equal to the circumference, another kind of wave traveling at rotational speed near the rotor rotation was also detected. Furthermore, in 1998 Weigl [36] showed that a single-

stage high speed compressor could drive stall inception waves at even 150% of the rotor rotation. Paduano, et al. [13] stated that these high speed modes are related to the flow compressibility which cannot be described in Greitzer & Moore model [37-38]. More in-depth explanation is not available. In brief, the prediction result in the present case is reasonable and it is obvious that compressibility is indispensable to complete and precise physical expression in a flow stability model, especially for the practical high speed flow.

4.1.2. Sensitivity of casing treatment on the stall inception

In the principle of this work, the novel casing treatment results in soft boundary condition and has the ability to enhance the stability of the system of fan/compressors. So, numerical test is conducted to check whether different configurations of such casing treatment in the model has the ability to turn the unstable point under the solid casing condition into a stable region, i.e., emphasis is placed on numerically studying the sensitivity of different design parameters of casing treatment on the stall inception of axial flow fan/compressors. The chosen point is an unstable point in the theoretical prediction, which corresponds to a flow rate coefficient at 0.375. The variable parameters of the configuration are the length of the casing treatment, the height of the backchamber, the open area ratio of the perforated plate and the bias flow rate through the apertures, which represent the effect of the recirculation flow in the casing treatment at the impedance boundary condition.

Figures 5-8 show the results for the stability prediction with the casing treatment at 70% design rotational speed. The vertical coordinates stand for the imaginary part of the perturbation frequency, which determines whether the system is stable or not. The results are shown in four different figures, in which one of the four parameters is adjusted while the others are unchanged.

It is found that the change of any parameter of the

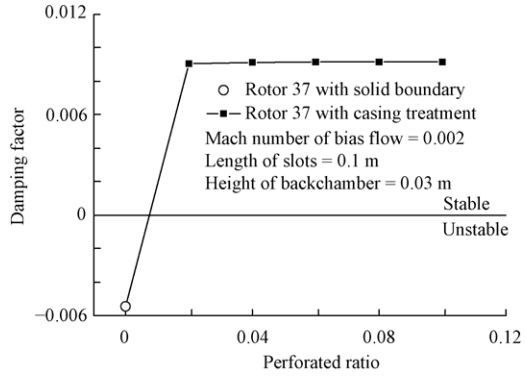

Fig. 5 Effect of open area ratio on the stability of the compressor of NASA Rotor 37 at 70% design rotational speed, mode number m=1.

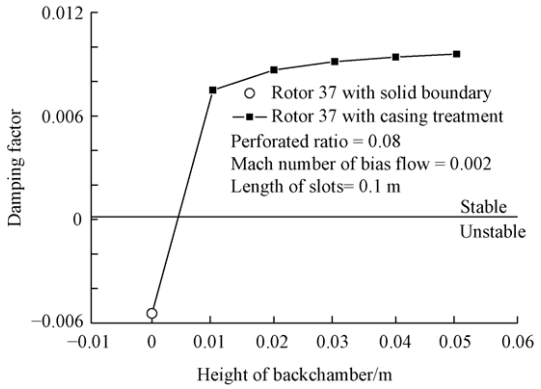

Fig. 6 Effect of height of backchamber on the stability of the compressor of NASA Rotor 37 at 70% design rotational speed, mode number m=1.

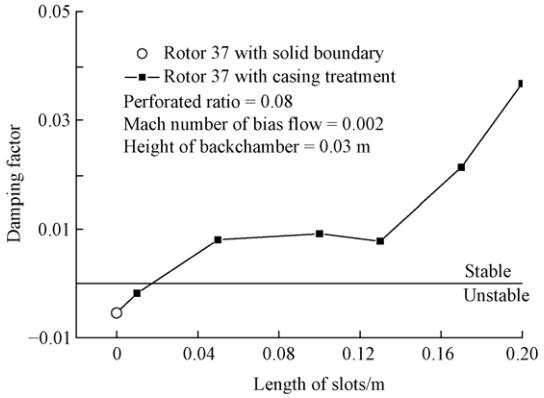

Fig. 7 Effect of length of casing treatment on the stability of the compressor NASA Rotor 37 at 70% design rotational speed, mode number m=1.

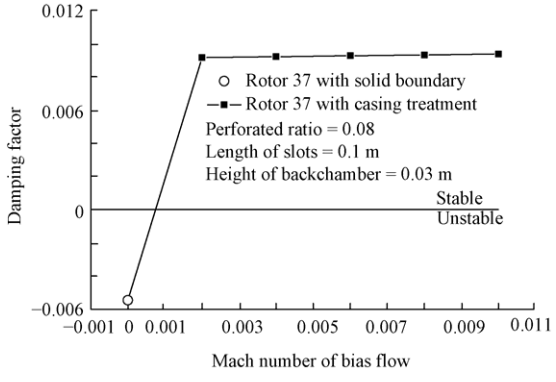

Fig. 8 Effect of Mach number of bias flow through the slots on the stability of the compressor NASA Rotor 37 at 70% design rotational speed, mode number m=1.

casing treatments will change all the stall inception from the unstable to the stable state. Obviously, as shown in Fig. 7, backchamber of enough length is necessary to stabilize the stall inception point. Besides, due to various restrictions to casing treatment size, the ranges of these parameters do not allow being arbitrarily decided, and a reasonable combination of these parameters is required.

4.2. Low speed TA36 Fan at design rotational speed

4.2.1. Experimental investigations and various comparisons for stall inception

Some experimental investigations of rotating stall are conducted on a low speed TA36 Fan in Beihang University, which is shown in Fig. 9, and the main design parameter of which is displayed in Table 1 and Table 2. This fan is equipped with accurate-regulating bleed valves, which can accurately move the operating point near stall and quickly move away from stall. All the steady-state operating characteristics of the compressors are gained using standard time-averaged instrumentation in this test rig.

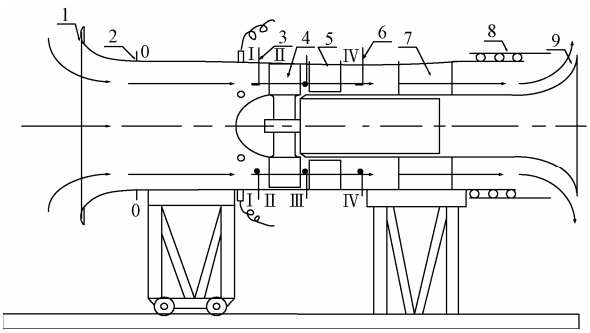

1—Flow tube; 2—Measurement point of wall static pressure; 3—Measurement point of inlet total pressure; 4—Rotor; 5—Stator; 6—Measurement point of outlet total pressure and static pressure; 7—Motor; 8—Struts; 9—Outlet adjusting mechanism.

Fig. 9 Schematic of TA36 Fan.

Table 1 Geometrical parameters for TA36 Fan

Parameter	Rotor	Stator
No. of blades	20	27
Tip diameter/mm	600	600
Hub to tip ratio	0.577	0.669
Tip stagger angle/(°)	45	0

Table 2 Aerodynamic parameters for TA36 Fan

Parameter	Value	Parameter	Value
Mass flow/(kg · s^{-1})	6.5	Design speed/(kg · s^{-1})	2 900
Efficiency/%	85	Total pressure ratio	1.022
Stall margin/%	15.5	Total pressure rise/Pa	2 000

Figure 10 shows the time history of the wall static pressure as measured by all eight sensors about the circumference on a magnified scale during the stalling transient, and regular disturbances can be observed here for an inconsiderable (short) time before the stall. The input data (see Fig. 11) is obtained from the throttling experiment on this fan, and the prediction result is given in Fig. 12. It should be noted that the point corresponding to the smallest mass flow is just the stall point in the experiment. So, the relative error between the measured and predicted critical point is less than 1%, and the relative speed at the stall inception point is approximately 63% of the rotor rotational speed which is quite close to the measured precursor rotating speed, i.e., 58% as shown in Fig. 10.

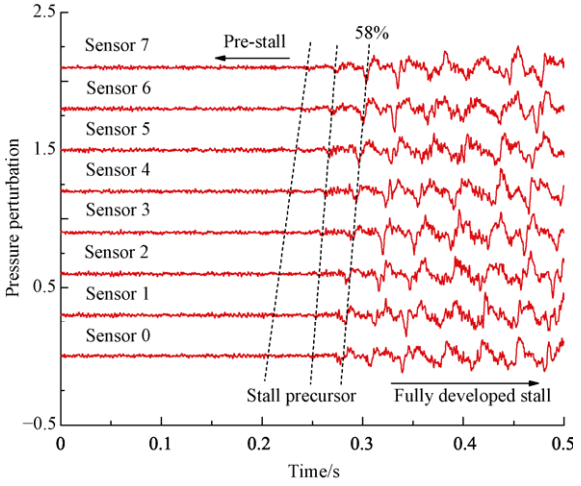

Fig. 10 Measured time traces of wall static pressure during transients into rotating stall on TA36 Fan at 100% rotational speed.

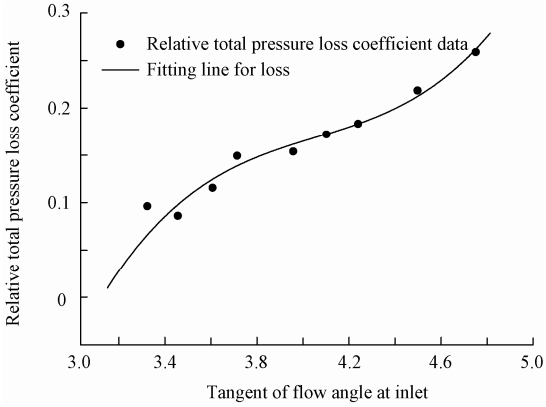

Fig. 11 Relative total pressure loss coefficient data and fitting line of a low speed axial flow compressor TA36 Fan at 100% rotational speed.

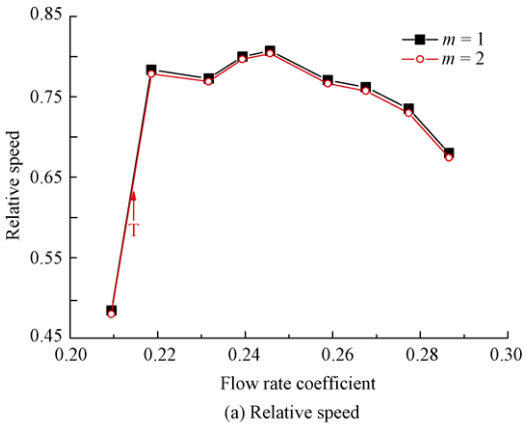

(a) Relative speed

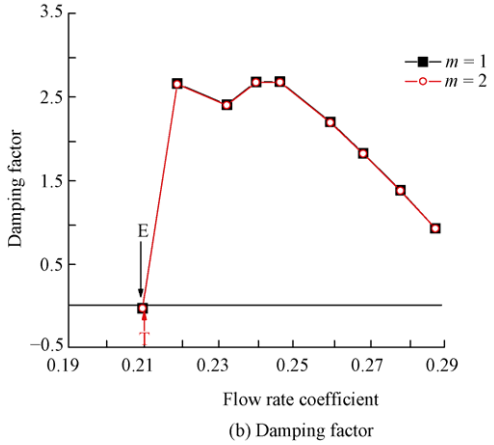

Fig. 12 Stability prediction of a low speed axial flow compressor TA36 Fan.

4.2.2. Sensitivity of casing treatment on stall inception

Figures 13-16 show how the stall inception varies with the design parameters of casing treatment. It is seen that the optimum combination of various parameters can be chosen in terms of these numerical analyses. Obviously, as shown in Fig. 15, it is not true that more large configuration parameters of casing treatment make the system of fan/compressors more stable. A reasonable combination of these parameters is required

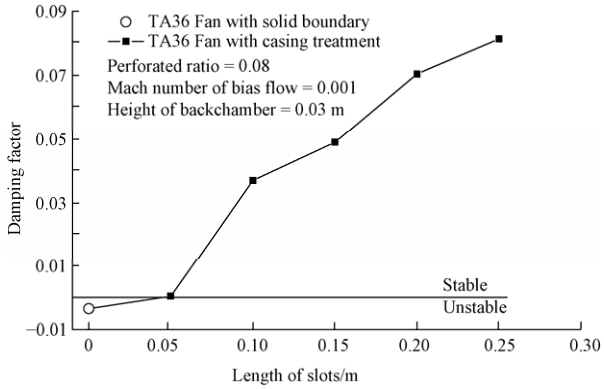

Fig. 13 Effect of length of casing treatment of on the stability of TA36 Fan, mode number m=1.

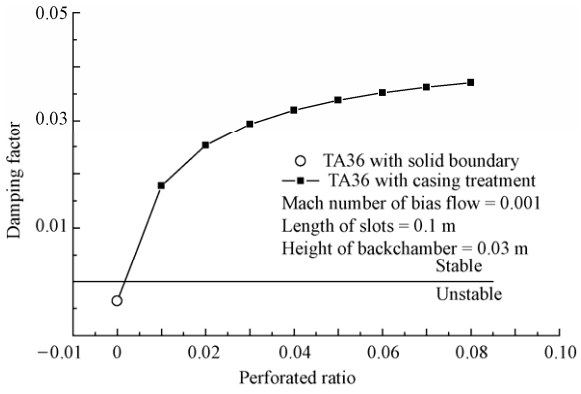

Fig. 14 Effect of open area ratio on the stability of TA36 Fan, mode number m=1.

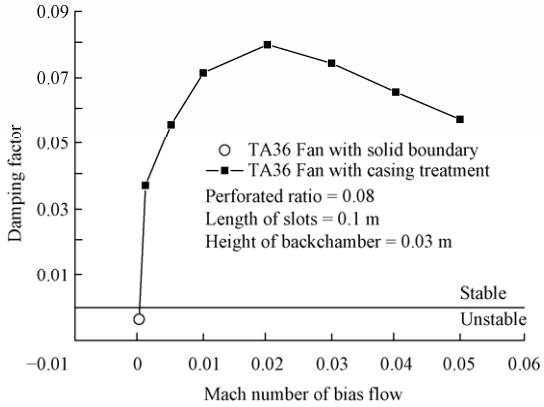

Fig. 15 Effect of Mach number of bias flow through the slots on the stability of TA36 Fan, mode number m=1.

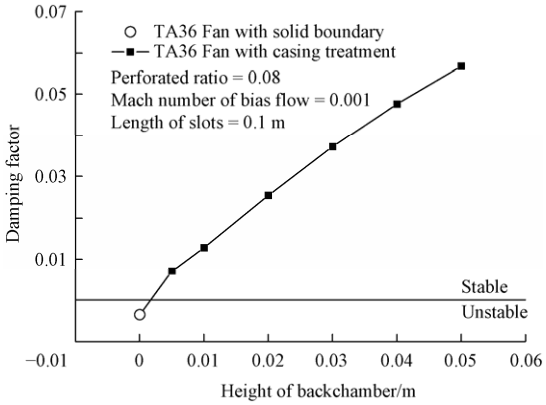

Fig. 16 Effect of height of backchamber on the stability of TA36 Fan, mode number m=1.

for the stability of the whole system. Besides, for unsteady physical process, it is not appropriate to roughly draw conclusion about the stall inception just by numerical convergence of steady CFD calculation. So it is suggested that the input data to this model prediction could be derived by CFD, and in this way the stability model can be applied to determining the stall margin during design stage of multi-stage fan/compressors. Such possibility for further application of this work is in progress.

5. Conclusions

1) A three-dimensional compressible flow stability model of multi-stage compressors including a finite large radius duct configuration is presented. Unlike the previous models concerning flat plate simplification for the actual annular duct, this model does not artificially decompose the radial modes, i.e., the eigenvalue solution for a coupled multi radial modes perturbation in a fan/compressors system is derived.

2) Two numerical validation cases show that this stability model can provide a reasonable prediction for the stall inception point for both low and high subsonic

fan/compressors with solid casing boundary, and a good agreement between relative speed and measured data can be achieved. Compared with the previous models considering a liner cascade with tip and hub plates, more accurate prediction results are obtained.

3) A mathematical model of a novel casing treatment is included in the stability model, which consists of backchamber and perforated plate. In contrast to the conventional recess casing treatment with more than 50% open area ratio, such casing treatment with very low open area ratio is aimed at affecting the evolution of the stall precursors for the stall margin improvement.

4) The sensitivity of the novel casing treatment on the stall inception is verified numerically. Theoretically it is possible to design a kind of advanced casing treatment with a reasonable combination of configuration parameters to suppress the stall precursor, which can result in the stall margin improvement without the obvious efficiency loss of fan/compressors.

5) It is suggested that extracting the input parameters from steady CFD calculation may be helpful to guarantee or check enough stall margin of fan/compressors during design phase.

References

[1] Emmons H W, Pearson C E, Grant H P. Compressor surge and stall propagation. Transactions of the ASME 1955; 79(4): 455-469.

[2] Nenni J P, Ludwig G R. A theory to predict the inception of rotating stall in axial flow compressors. AIAA-1974-528, 1974.

[3] Ludwig G R, Nenni J P. Basic studies of rotating stall in axial flow compressors. AFAPL-TR-79-2083, 1979.

[4] Stenning A H. Rotating stall and surge. Journal of Fluids Engineering 1980; 102(1): 14-20.

[5] Sun X F. On the relation between the inception of rotating stall and casing treatment. AIAA-1996-2579, 1996.

[6] Sun X F, Sun D K, Yu W W. A model to predict stall inception of transonic axial flow fan/compressors. Chinese Journal of Aeronautics 2011; 24(6): 687-700.

[7] Crook A J, Greitzer E M, Tan C S, et al. Numerical simulation of compressor endwall and casing treatment flow phenomena. Journal of Turbomachinery 1993; 115(3): 501-511.

[8] Gorrel S E, Russler P M. Stall inception in a high-speed low aspect ratio fan including the effects of casing treatments. ASME-GT-332, 1994.

[9] Kang C S, Mckenzie A B, Elder R L. Recessed casing treatment effects on fan performance and flow field. ASME-GT-197, 1995.

[10] Bard H. Fan stability by anti-stall in tunnels and industrial process ventilation, turbo compressor and fan stability. Fluid Machinery Committee of Institution of Mechanical Engineer. 1993.

[11] Azimian A R, Elder R L, McKenzie A B. Application of recess vaned casing treatment to axial flow fan. Journal of Turbomacinery 1990; 112(1): 145-150.

[12] Ziabasharhagh M, McKenzie A B, Elder R L. Recess vane passive stall control. ASME-GT-36, 1992.

[13] Paduano J D, Greitzer E M, Epstein A H. Compression system stability and active control. Annual Review of Fluid Mechanics 2001; 33: 491-517.

[14] Tan C S, Day I, Morris S, et al. Spike-type compressor stall inception, detection, and control. Annual Review of Fluid Mechanics 2010; 42: 275-300.

[15] Osborn W M, Lewis G W, Heidelberg L J. Effect of several porous casing treatments on stall limit and on overall performance of axial-flow compressor rotor. NASA TN D-6537, 1971.

[16] Osborn W M, Moore R D. Effect of casing treatment on overall performance of axial-flow transonic fan stage with pressure ratio of 1.75 and tip solidity of 1.5. NASA TM X-3477, 1977.

[17] Takata H, Tsukuda Y. Stall margin improvement by casing treatment—its mechanism and effectiveness. ASME Journal of Engineering for Power 1979; 99: 121-133.

[18] Greitzer E M, Nikkanen J P, Haddad D E, et al. A fundamental criterion for the application of rotor casing treatment. Journal of Fluid Engineering 1979; 101(2): 237-243.

[19] Smith G D J, Cumpsty N A. Flow phenomena in compressor casing treatment. Journal of Engineering for Gas Turbines and Powers 1984; 106: 533-541.

[20] Sun D K, Hou R W, Sun X F. An experimental investigation of rotating stall margin improvement with unsteady casing treatments. Journal of Aerospace Power 2008; 23(4): 662-670. [in Chinese]

[21] Sun D K, Sun X F. An experimental study on inhibition of unsteady casing treatment on stall inception. Journal of Aerospace Power 2008; 23(4): 671-679. [in Chinese]

[22] Brazier-Smith P R, Scott J F. On the determination of the dispersion equations by use of winding number integrals. Journal of Sound and Vibration 1991; 145(3): 503-510.

[23] Ivansson S, Karasalo I. Computation of modal numbers using an adaptive winding-number integral method with error control. Journal of Sound and Vibration 1993; 161(1): 173-180.

[24] Bechert D W. Sound absorption caused by vorticity shedding, demonstrated with a jet flow. Journal of Sound and Vibration 1980; 70(3): 389-405.

[25] Howe M S. Theory of vortex sound. Cambridge: Cambridge University Press, 2002.

[26] Howe M S. On the theory of unsteady high Reynolds number flow through a circular aperture. Proceedings of the Royal Society London A366. 1979; 205-223.

[27] Jing X D, Sun X F. Wall thickness influence on the impedance of perforated plates with bias flow. AIAA Journal 2000; 38(9): 1573-1578.

[28] Jing X D, Sun X F. Sound-excited flow and acoustic nonlinearity at an orifice. Physics of Fluids 2002; 14(1): 268-276.

[29] Jing X D, Sun X F, Wu J, et al. Effect of grazing flow on the acoustic impedance of an orifice. AIAA Journal 2001; 39(8): 1478-1484.

[30] Sun X F, Jing X D, Zhang H, et al. Effect of grazing-bias flow interaction on acoustic impedance of perforated plates. Journal of Sound and Vibration 2002; 254(3): 557-573.

[31] Peat K S, Ih J G, Lee S H. The acoustic impedance of a circular orifice in grazing mean flow: comparison with theory. Journal of the Acoustical Society of America 2003; 114(6): 3076-3086.

[32] Namba M, Fukushige K. Application of the equivalent surface source method to the acoustics of duct systems with non-uniform wall impedance. Journal of Sound

and Vibration 1980; 73(1): 125-146.
[33] Sun X F, Wang X Y, Du L, et al. A new model for the prediction of turbofan noise with the effect of locally and non-locally reacting liners. Journal of Sound and Vibration 2008; 316(1-5): 50-68.
[34] Moore R D, Reid L. Performance of single-stage axial flow transonic compressor with rotor and stator aspect ratios of 1.19 and 1.26, respectively, and with design pressure ratio of 2.05. NASA TP-2001, 1980.
[35] Tryfonidis M, Etchevers O, Paduano J D, et al. Pre-stall behavior of several high-speed compressors. Journal of Turbomachinery 1995; 117(1): 62-80.
[36] Weigl H J. Active stabilization of rotating stall and surge in a transonic single-stage axial compressor. Journal of Turbomachinery 1998; 120(4): 625-636.
[37] Greitzer E M, Moore F K. A theory of post-stall transients in axial compression systems: part I—development of equations. Journal of Engineering for Gas Turbine and Power 1986; 108(1): 68-76.
[38] Greitzer E M, Moore F K. A theory of post-stall transients in axial compression systems: part II—application. Journal of Engineering for Gas Turbine and Power 1986; 108(2): 231-239.

Biographies:

LIU Xiaohua received his B.S. degree from Beihang University in 2007, and then became a Ph.D candidate there. His main research interest is flow stability of fan/compressor.
E-mail: Liuxh@sjp.buaa.edu.cn

SUN Dakun received Ph. D. degree from Beihang University in 2010. His main research interest is flow stability of compressor.
E-mail: renshengming@sjp.buaa.edu.cn

SUN Xiaofeng is a professor in Beihang University. His main research interests are flow stability of fan/compressor and combustion, acoustic design of modern passenger aircraft and aeroacoustics.
E-mail: sunxf@buaa.edu.cn

WANG Xiaoyu received Ph. D. Degree from Beihang University in 2010. Her main research interest is duct aeroacoustics.
E-mail: bhwxy@sjp.buaa.edu.cn